He, Ne and Ar 'snapshot' of the subcontinental lithospheric mantle from CO2 well gases

Chemical Geology xxx (xxxx) xxx–xxx

Contents lists available at ScienceDirect

Chemical Geology

journal homepage: www.elsevier.com/locate/chemgeo

He, Ne and Ar 'snapshot' of the subcontinental lithospheric mantle from CO_2 well gases

Stuart M.V. Gilfillan[a,*], Chris J. Ballentine[b]

[a] School of Geosciences, University of Edinburgh, James Hutton Road, Edinburgh EH9 3FE, UK
[b] Department of Earth Sciences, South Parks Road, Oxford OX1 3AN, UK

ARTICLE INFO

Keywords:
Colorado Plateau
Noble gases
Helium
Neon
Argon
Lithospheric mantle
Well gases
Magmatic

ABSTRACT

The subcontinental lithospheric mantle (SCLM) constitutes a significant portion of the upper mantle sourcing magmatic volatiles to the continents above, yet its geochemical signature and evolution remain poorly constrained. Here we present new interpretation of noble gas datasets from two magmatic CO_2 fields in the SW US, namely Bravo Dome and Sheep Mountain, which provide a unique insight into the volatile character of the SCLM sourcing the Cenozoic volcanism in the region. We identify that reduction of $^3He/^4He_{mantle}$ ratio within the Sheep Mountain CO_2 field can be attributed to radiogenic production within the SCLM. Using a Reduced Chi-Squared minimisation on the variation of derived $^4He/^{21}Ne_{crust}$ ratios within samples from the Sheep Mountain field, combined with a radiogenically raised $^{21}Ne/^{22}Ne_{mantle}$ end member, we resolve $^3He/^4He_{mantle}$ ratios of 2.59 ± 0.15 to 3.00 ± 0.18 R_a. These values correspond with a $^{21}Ne/^{22}Ne_{mantle}$ value of 0.136. Using these $^3He/^4He_{mantle}$ end member values with $^{21}Ne_{mantle}$ resolved from Ne three component analysis, we derive the elemental $^3He/^{22}Ne_{mantle}$ of 2.80 ± 0.16 and radiogenic $^4He/^{21}Ne^*_{mantle}$ range of 1.11 ± 0.11 to 1.30 ± 0.14. A second Reduced Chi-Squared minimisation performed on the variation of $^{21}Ne/^{40}Ar_{crust}$ ratios has allowed us to also determine both the $^4He/^{40}Ar_{mantle}$ range of 0.78 to 1.21 and $^{21}Ne/^{40}Ar_{mantle}$ of 7.66 ± 1.62 to 7.70 ± 1.54 within the field. Combining these ratios with the known mantle production ranges for $^4He/^{21}Ne$ and $^4He/^{40}Ar$ allows resolution of the radiogenic He/Ne and He/Ar ratios corresponding to the radiogenically lowered $^3He/^4He_{mantle}$ ratios. Comparing these values with those resolved from the Bravo Dome field allows identification of a clear and coherent depletion of He to Ne and He to Ar in both datasets. This depletion can only be explained by partial degassing of small melt fractions of asthenospheric melts that have been emplaced into the SCLM. This is the first time that it has been possible to resolve and account for both the mantle He/Ne and He/Ar ratios within a SCLM source. The data additionally rule out the involvement of a plume component in the mantle source of the two gas fields and hence any plume influence on the Colorado Plateau Uplift event.

1. Introduction

The subcontinental lithospheric mantle (SCLM) can be defined as the basal part of the Earth's outer ridged mechanical boundary layer, where heat loss occurs by conduction (Day et al., 2015). The SCLM constitutes a significant portion of the upper mantle, making up ~2.5% by volume of the total mantle (Pearson and Wittig, 2008). The SCLM sources magmatic volatiles to the continents above, yet its geochemical signature and evolution remain poorly constrained. Traditionally, upper mantle characteristics have been deduced from the more conveniently sampled convective mantle, via mid-ocean ridge basalts (MORB). The SCLM has been physically isolated from this convective portion of the upper mantle for over 1×10^9 year (Ga) time scales (McDonough, 1990) as indicated by > 2 Ga Os isotope model ages in SCLM peridotites (Pearson et al., 1995a; Pearson et al., 1995b; Walker et al., 1989). This isolation has resulted in the SCLM developing its own unique isotopic, major and trace element signature (McDonough, 1990). The SCLM potentially contains a significant quantity of noble gases and other trace elements and re-entrainment of this material into the deeper mantle may contribute to the characteristic mantle signature sampled at ocean islands (Gautheron and Moreira, 2002).

Noble gases, and the $^3He/^4He$ ratio in particular, provide vital information about the character and processes controlling the mantle volatile source. Previous studies have identified that the isotopic ratio of He within the SCLM is more radiogenic than that of the MORB source mantle-which is typically cited to be 8 ± 1 R_a (Day et al., 2015; Day

* Corresponding author.
E-mail address: stuart.gilfillan@ed.ac.uk (S.M.V. Gilfillan).

http://dx.doi.org/10.1016/j.chemgeo.2017.09.028
Received 1 December 2016; Received in revised form 28 July 2017; Accepted 19 September 2017

et al., 2005; Dunai and Baur, 1995; Dunai and Porcelli, 2002; Porcelli et al., 1987). This is reflected in the latest $^3He/^4He$ compilation estimate which cites a range of 6.1 ± 0.9 R_a for the SCLM (Gautheron and Moreira, 2002). A recent study of exsolving free gases by Bräuer et al. (2016) measured $^3He/^4He$ ratios from 4.95 to 6.32 R_a in the westernmost part of the Pannonian Basin near the Austria/Slovenia border, corroborating earlier measurements of the more radiogenic than MORB signature of the SCLM. The origin of this radiogenic He has proved to be enigmatic and several explanations have been proposed including; alteration of the MORB source mantle by either addition of sediments (Dunai and Baur, 1995); isolation and ageing (Reid and Graham, 1996); or regional low $^3He/^4He$ plume sources (Duncan and Richards, 1991; White and McKenzie, 1995).

The Ne and Ar isotopic composition of the SCLM are even less well constrained, with previous studies documenting small anomalies compared to air values (Barford et al., 1999; Matsumoto et al., 1998) but also a small mantle component similar in character to MORB (Gautheron et al., 2005). These observations have been explained by atmospheric contamination or the recycling of an atmospheric component back into the lithospheric mantle (Gautheron et al., 2005). A number of recent studies (Holland and Ballentine, 2006; Kendrick et al., 2013; Kendrick et al., 2011; Sumino et al., 2010) have proposed that atmospheric derived noble gases can be recycled into the mantle via subduction. Matsumoto et al. (2001) proposed that the SCLM can potentially store these atmospheric noble gases. This issue is critical to rare gas budgets, as the SCLM can be delaminated and recycled back into the convecting mantle (Seber et al., 1996), and thus potentially help explain the numerous OIB which exhibit lower or MORB like $^3He/^4He$ ratios. These include OIB's observed at the Canary Islands (Day and Hilton, 2011), the Comores (Class et al., 2005), the Cook-Austral Archipelago (Hanyu and Kaneoka, 1997; Hanyu et al., 2011), the Azores (Moreira et al., 2012) and St. Helena (Barfod et al., 1999).

Our current knowledge of the characteristics of the SCLM has been deduced from magmas derived from melting of this portion of the mantle and from xenoliths trapped by rapidly rising magmas. However, typically magmas that reach the surface subaerially are strongly degassed and apart from occasional phenocrysts, do not contain a significant quantity of noble gases (Dodson et al., 1998; Dunai and Porcelli, 2002). Hence, the vast majority of data regarding the SCLM has been obtained from analysis of ultramafic xenoliths sourced from continental volcanic provinces (Day et al., 2015). Unfortunately, whilst some volcanic localities allow local mantle $^3He/^4He$ to be determined from these xenoliths, suitable samples are not always available, and air contamination of this sample type often precludes resolution of the heavy mantle-derived noble gases.

Magmatic CO_2 well gases provide a resource that enables the $^3He/^4He$, heavy noble gas isotope and relative abundance determination of the mantle source to be resolved (Ballentine et al., 2005; Holland and Ballentine, 2006). Primordial noble gas isotopes have been studied in well gases since 1961 (Boulos and Manuel, 1971; Butler et al., 1963; Caffee et al., 1999; Hennecke and Manuel, 1975; Phinney et al., 1978; Smith and Reynolds, 1981; Staudacher, 1987; Zartman et al., 1961), but until recently their use in investigating the SCLM in detail has been limited. Here we present noble gas analyses from magmatic CO_2 well gases in the SW US that provide a unique insight into the volatile character of the SCLM sourcing the Cenozoic volcanism in the region. For the first time, we have been able to resolve the mantle He, Ne and Ar ratios of the mantle source beneath these two natural magmatic CO_2 reservoirs. Combining our new data from the Sheep Mountain CO_2 field with previous measurements from the Bravo Dome CO_2 field (Ballentine et al., 2005) suggests that the process responsible for reducing the $^3He/^4He_{mantle}$ ratio within the SCLM is radiogenic production within the mantle. This permits critical analysis of models proposed to account for the SCLM evolution and volatile origin in greater detail than has been previously possible.

2. Tectonic setting of Colorado Plateau and Rocky Mountain natural CO_2 reservoirs

The Colorado Plateau is a massive, high-standing tectonic block located in the south-western US, centred on the Four Corners of the states of Colorado, New Mexico, Utah, and Arizona. It is abruptly flanked to the east by the Rio Grande rift and the majestic Rocky Mountains, the result of at least 2 km of uplift during the Laramide Orogeny and later Cenozoic uplifts (Parsons and McCarthy, 1995). To the south it is bounded by the Mogollon Rim and on the west by the Basin and Range Province, the result of pervasive tectonic extension that began around 17 Ma in the Early Miocene time.

2.1. Cenozoic volcanism and the Colorado Plateau Uplift event

In the late Cenozoic the cessation of subduction along the Pacific margin triggered extensive basic magmatic activity and accompanying lithosphere extension, block faulting and local uplift across the western US (Becker et al., 2014; Fitton et al., 1991). These events had a dramatic effect on the Colorado Plateau which was uplifted some 2 km (Erdman et al., 2016), with the most recent uplift event raising the south-western margin of the Plateau by approximately 1 km, between 6 and 1 Ma (Parsons and McCarthy, 1995). However, it is the lack of significant deformation of the region that is even more significant, especially given the rapid nature of the uplift event. Both the Rio Grande rift and the Basin and Range province have experienced similar degrees of uplift and have suffered extensive compression and internal faulting, whilst the Colorado Plateau has remained a rigid block, resistant to significant deformation (Becker et al., 2014; Erdman et al., 2016; Parsons and McCarthy, 1995).

The scale of the uplift event and the dominance of basaltic magmatism throughout imply some degree of mantle influence in the process, though the exact mechanism remains highly contentious. Several mechanisms have been proposed including; crustal thickening caused by horizontal compression (Dilek and Moores, 1999); dynamic topography (Moucha et al., 2008), thermal expansion due to a mantle plume (Fitton et al., 1991; Wilson, 1973); a reduction in the density of the mantle caused by physical thinning or thermal expansion of the lithosphere lid (Roy et al., 2009) or by the presence of a plume component (Parsons and McCarthy, 1995); and complete or partial lithosphere delamination of the Farallon Plate following flat slab subduction (Beghoul and Barazangi, 1989; Bird, 1979; Humphreys, 1995; Levander et al., 2011; Thompson and Zoback, 1979; Zandt et al., 1995).

2.2. Regional geology of Colorado Plateau and Rocky Mountain reservoirs

Within the Colorado Plateau and surrounding Rocky Mountain region there are at least nine producing or abandoned gas fields that contain up to 2800 billion m^3 of natural CO_2 (Allis et al., 2001; Miocic et al., 2013; Miocic et al., 2016; NETL, 2014). In this paper we detail the results from two separate gas fields, namely Sheep Mountain (Huerfano County, CO), and Bravo Dome (Harding County, NM), both of which contain extremely high concentrations of magmatic CO_2 (> 95% CO_2). The background geology and location of these sites is outlined in detail in Gilfillan et al. (2008).

2.2.1. Sheep Mountain

The Sheep Mountain gas field is located at the northern end of the Raton Basin, some 45 km northwest of the town of Walsenburg, south central Colorado. This region was extensively tilted and folded as a result of uplift to the west during by the Laramide Orogeny in the late Cretaceous-early Tertiary time (Woodward, 1983). As a result of this event, large volumes of lava were extruded from vents along the Sierra Grande arch, within the Raton Basin and on the eastern margin of the basin. Intrusive activity accompanied these volcanics, producing extensive sills and laccoliths including the distinctive peaks of Little Sheep

Mountain, Sheep Mountain and Dike Mountain. The nearest intrusive to the field is the Sheep Mountain – Little Sheep Mountain laccolith, which consists of intermediate-acidic igneous rocks and trends north-northwest covering an area of approximately 13 km^2 (Johnston, 1959; Roth, 1983; Woodward, 1983).

2.2.2. Bravo Dome

The Bravo Dome field (originally named the Bueyeros field) is located south of Cortez in Harding County, northeastern New Mexico. It is a large field (2000 km^2) which consists of a northwest trending anticlinal nose situated on the spur of the Sierra Grande arch (Baines and Worden, 2004). The field is bounded by the Tucumari basin to the south and the Dalhart Basin to the north (Baars, 2000; Johnson, 1983). CO_2 from the field has been studied since the 1960s (Boulos and Manuel, 1971; Butler et al., 1963; Hennecke and Manuel, 1975; Zartman et al., 1961). Phinney et al. (1978) reported the first ^3He excess in the gas, which they attributed to a primordial mantle source. This was confirmed by Staudacher (1987) who showed that the noble gas pattern from CO_2 within the field was indistinguishable from that of fresh MORB glasses and this has been reinforced by the recent studies of Caffee et al. (1999), Ballentine et al. (2005) and Holland and Ballentine (2006). CO_2 is believed to have migrated from vents associated with the nearby Rio Grande rift volcanic activity, via deep seated faults that cut through the fractured basement below the reservoir (Baines and Worden, 2004). Known volcanic activity in the region was thought to date from 100,000 to 8000 years ago (Broadhead, 1998), though recent work has more accurately constrained the latest emplacement of hot gases into the reservoir to be between 1.2 and 1.5 Ma (Sathaye et al., 2014) suggesting the field filled relatively recently.

3. Sample collection and analytical techniques

Samples from the two gas fields were collected directly from producing wellheads that tap the natural gas reservoirs. Sample localities were chosen on site from available producing wells to provide a wide range of depth and spatial distribution across the fields. Samples were collected via the conventional ¾-inch National Pipe Thread (NPT) sample port of the well head using 'Swagelok©' 300 ml stainless steel sampling cylinders sealed at both ends with high-pressure valves as outlined in detail in previous work (Gilfillan et al., 2008; Holland and Gilfillan, 2013).

^4He, ^{20}Ne, ^{40}Ar, ^{84}Kr, ^{132}Xe, $^3He/^4He$, $^{20}Ne/^{22}Ne$, $^{21}Ne/^{22}Ne$, $^{40}Ar/^{36}Ar$ and $^{130}Xe/^{136}Xe$ for Sheep Mountain were determined at the University of Manchester using an all metal purification line and a MAP 215 mass spectrometer using the procedures outlined in Gilfillan et al. (2008). Blank levels were negligible compared to original sample size for all isotopes except ^{20}Ne, which was typically < 1%. The Bravo Dome samples documented in this study were analysed at ETH (Eidgenössische Technische Hochschule; Federal Institute of Technology), and analytical methods are documented in Ballentine et al. (2005).

4. Results

A total of 32 deep CO_2 well gas samples from the two gas fields were analysed as part of a comprehensive study of CO_2 reservoirs and natural seeps in the Colorado Plateau and Rocky Mountain regions (Gilfillan et al., 2008). Table 1 documents the sample location, producing formation and noble gas isotopic composition and abundance measurements. More recent sample collection and analysis by Holland and Ballentine (2006) expanded the mantle rich portion of the Bravo Dome dataset. However, we use earlier values determined at ETH by Ballentine et al. (2005) which have greater crustal contributions, and therefore provide a clearer resolution of the crustal end member present in the field.

4.1. Helium

$^3He/^4He$ values from the Bravo Dome field exhibit a coherent variation from 0.764 to 4.07 R_a on moving eastwards within the field (4.26 R_a has been measured in a previous study) (Ballentine et al., 2005). This corresponds with a significant decrease in both ^3He (Table 1) and ^4He concentrations (Fig. 1), highlighting that the high mantle $^3He/^4He$ input value is being reduced by the addition of crustal radiogenic ^4He to the west of the field. This is a stark contrast to the $^3He/^4He$ values from the Sheep Mountain field that are remarkably uniform and predominantly lower, varying from 0.916 up to 1.06 R_a (Fig. 1). No spatial control on this variation exists indicating that the field has either been homogenized over time or that crustal radiogenic ^4He and mantle derived ^3He were well mixed prior to entering the gas field.

Absolute ^3He concentrations in both fields are high, ranging from 4.96 to 9.84 $\times 10^{-10}$ $cm^3(STP)cm^{-3}$ within Sheep Mountain and 2.10 to 4.34 $\times 10^{-10}$ $cm^3(STP)cm^{-3}$ in Bravo Dome, with both falling directly within the pure magmatic CO_2 range of 1×10^{-10} and 5×10^{-10} $cm^3(STP)cm^{-3}$ (Ballentine et al., 2001; Marty and Jambon, 1987). Measured $CO_2/^3He$ ratios from both fields also plot within the magmatic range of 1×10^9–1×10^{10} confirming that the CO_2 contained in the reservoirs has a predominantly mantle origin.

4.2. Neon

Within the Bravo Dome field both the variation in $^{20}Ne/^{22}Ne$ from 9.93 ± 0.09 to 11.88 ± 0.05 and $^{21}Ne/^{22}Ne$ values from 0.0501 ± 0.0003 to 0.0579 ± 0.0005 exhibit a similar spatial correlation as that observed in $^3He/^4He$ (Fig. 1). Neon isotope measurements from Sheep Mountain exhibit a significantly larger variation than those observed in the $^3He/^4He$ ratios (Fig. 2). Measured $^{20}Ne/^{22}Ne$ values vary between 9.84 ± 0.03 and 10.29 ± 0.08. $^{21}Ne/^{22}Ne$ varies between 0.031 ± 0.0003 and 0.614 ± 0.0003, illustrating a clear mixing relationship with the air sourced from the formation water present in the reservoir. This is indicated by a reduction of the $^{21}Ne/^{22}Ne$ ratio with a corresponding increase of air-derived ^{20}Ne concentrations (Table 1).

As Ne is derived from three isotopically distinct sources, (namely the crust, mantle and air), the contribution of each of these sources to any sample can be resolved using established techniques (Ballentine, 1997; Ballentine et al., 2002). This is because any sample that contains a mix of these components must plot within the envelope defined by the well-known $^{20}Ne/^{22}Ne$ and $^{21}Ne/^{22}Ne$ air and crust end members and the resolved mantle end member values of 12.5 for $^{20}Ne/^{22}Ne$ and 0.06 for $^{21}Ne/^{22}Ne$ (Ballentine et al., 2005).

Fig. 2 highlights the distinct crust/mantle/air mixing trends that can be observed in the Ne isotope data from the two fields. Sheep Mountain exhibits a clear mixing trend between air and a pre-mixed crust and mantle component. Bravo Dome, on the other hand, highlights mixing between an original mantle component and an air/crust mixture.

4.3. Argon

Bravo Dome $^{40}Ar/^{36}Ar$ vary from 4654 up to 22,492 and also exhibit the same coherent spatial variation as observed in both $^3He/^4He$ and $^{20}Ne/^{22}Ne$. $^{40}Ar/^{36}Ar$ in the Sheep Mountain field vary from 4400 to 21,200. A lowering of the $^{40}Ar/^{36}Ar$ ratio corresponding to increasing ^{36}Ar concentrations highlights mixing of an air component, derived from the formation water, with the gas within the reservoir.

Atmospheric contributions to ^{40}Ar can be resolved using the formula outlined by Ballentine et al. (2002) Eq. (1), assuming that all of the ^{36}Ar originates from the atmosphere. This is a valid assumption as ^{36}Ar production in the crust is small compared to the ambient background of atmosphere-derived ^{36}Ar introduced into the crust dissolved in groundwater and is usually neglected (Ballentine and Burnard, 2002).

Table 1
Sample location, noble gas isotope ratios and concentrations.

Field & $	Location Sec/Twp/Rge	$^{3}He/^{4}He$	$^{20}Ne/^{22}Ne$	$^{21}Ne/^{22}Ne$	$^{40}Ar/^{36}Ar$	^{4}He ($\times 10^{-4}$)cm^3(STP) cm^{-3}	^{20}Ne ($\times 10^{-8}$)cm^3(STP) cm^{-3}	^{40}Ar ($\times 10^{-4}$)cm^3(STP) cm^{-3}	^{84}Kr ($\times 10^{-10}$)cm^3(STP) cm^{-3}	^{130}Xe ($\times 10^{-12}$)cm^3(STP) cm^{-3}
Sheep Mtn										
8-2-P	2/9-28S/70W	0.981 (0.010)	10.14 (0.06)	0.0410 (0.0002)	13,839 (41)	3.13 (0.03)	1.47 (0.02)	1.67 (0.01)	2.96 (0.25)	4.76 (0.08)
2-10-O	15/9-27S/70W	0.984 (0.012)	10.08 (0.05)	0.0377 (0.0002)	10,744 (39)	2.96 (0.03)	3.04 (0.03)	1.62 (0.01)	3.10 (0.30)	4.65 (0.08)
9-26	26/9-27S/70W	0.934 (0.014)	10.19 (0.08)	0.0461 (0.0003)	16,486 (67)	2.95 (0.03)	0.613 (0.009)	1.57 (0.02)	4.19 (1.91)	4.11 (0.07)
2-9-H	9/9-27S/70W	0.945 (0.019)	10.11 (0.06)	0.0312 (0.0003)	4378 (21)	3.07 (0.03)	9.77 (0.10)	1.39 (0.01)	5.54 (1.14)	8.93 (0.15)
3-15-B	15/9-27S/70W	0.937 (0.016)	10.11 (0.06)	0.0375 (0.0003)	8745 (19)	2.90 (0.03)	1.54 (0.02)	1.60 (0.02)	9.85 (1.84)	6.50 (0.11)
4-13		0.942 (0.018)	10.20 (0.06)	0.0405 (0.0003)	17,292 (92)	3.47 (0.04)	1.11 (0.02)	2.08 (0.02)	4.58 (1.96)	5.63 (0.10)
4-26-E	26/9-27S/70W	1.024 (0.018)	10.29 (0.11)	0.0614 (0.0003)	21,203 (46)	3.15 (0.03)	0.442 (0.004)	1.73 (0.01)	7.16 (4.03)	4.47 (0.08)
3-23-D	22/9-27S/70W	0.988 (0.014)	10.15 (0.04)	0.0535 (0.0003)	16,956 (42)	3.17 (0.03)	0.579 (0.009)	1.84 (0.02)	8.48 (2.62)	3.27 (0.06)
7–35-L	2/9-28S/70W	0.916 (0.014)	10.23 (0.03)	0.0511 (0.0003)	17,590 (33)	3.06 (0.03)	0.749 (0.012)	1.56 (0.01)	5.36 (0.53)	5.22 (0.09)
2-35-C	26/9-27S/70W	0.963 (0.019)	10.29 (0.08)	0.0528 (0.0003)	16,566 (49)	2.87 (0.03)	0.573 (0.008)	1.57 (0.01)	2.71 (0.48)	4.79 (0.08)
1-15-C	15/9-27S/70W	0.967 (0.016)	9.94 (0.06)	0.0311 (0.0003)	5194 (30)	2.71 (0.03)	6.77 (0.10)	1.55 (0.02)	5.00 (2.09)	NM
3-4-O	9/9-27S/70W	0.937 (0.014)	9.93 (0.09)	0.0342 (0.0003)	4538 (10)	2.99 (0.03)	2.64 (0.03)	1.57 (0.01)	8.61 (0.54)	4.89 (0.09)
4-14-M	22/9-27S/70W	0.892 (0.015)	9.97 (0.06)	0.0404 (0.0003)	17,895 (173)	3.00 (0.03)	1.11 (0.01)	1.63 (0.02)	2.09 (0.52)	1.06 (0.18)
5-15-O	22/9-27S/70W	1.056 (0.015)	9.89 (0.06)	0.0319 (0.0003)	8720 (25)	2.92 (0.03)	4.33 (0.05)	1.51 (0.01)	3.69 (0.34)	5.44 (0.09)
4-4-P	9/9-27S/70W	0.970 (0.014)	10.15 (0.08)	0.0440 (0.0003)	16,010 (36)	2.52 (0.02)	1.31 (0.02)	1.60 (0.02)	2.73 (0.50)	5.52 (0.10)
5-9-A	9/9-27S/70W	1.006 (0.018)	10.15 (0.03)	0.0428 (0.0003)	17,813 (38)	2.94 (0.03)	1.28 (0.02)	2.06 (0.01)	3.05 (0.50)	3.15 (0.06)
1-1-J	2/9-28S/70W	0.908 (0.016)	9.84 (0.03)	0.0407 (0.0003)	12,037 (22)	2.16 (0.02)	0.878 (0.012)	1.66 (0.01)	5.29 (0.09)	NM
1-22-H	22/9-28S/70W	0.981 (0.017)	10.03 (0.02)	0.0401 (0.0003)	10,864 (69)	3.22 (0.03)	0.937 (0.013)	1.55 (0.01)	5.72 (0.11)	NM
Bravo Dome										
BD01	23/19N/34E	1.670 (0.008)	10.66 (0.03)	0.0562 (0.0003)	10,700 (314)	0.944 (0.012)	0.169 (0.002)	0.303 (0.003)	1.01 (0.02)	NM
BD02	32/21N/35E	0.764 (0.004)	9.96 (0.03)	0.0501 (0.0003)	4654 (41)	4.15 (0.05)	0.700 (0.007)	0.652 (0.006)	5.04 (0.14)	9.83 (0.40)
BD03	36/22N/34E	0.896 (0.004)	10.01 (0.01)	0.0515 (0.0001)	5342 (71)	3.31 (0.04)	0.521 (0.005)	0.536 (0.005)	3.24 (0.08)	NM
BD04	8/20N/34E	1.611 (0.008)	10.59 (0.04)	0.0541 (0.0004)	9886 (185)	9.61 (0.02)	0.181 (0.002)	0.286 (0.003)	1.03 (0.03)	2.09 (0.09)
BD05	34/20N/35E	0.965 (0.005)	9.93 (0.01)	0.0526 (0.0002)	5408 (38)	2.70 (0.04)	0.446 (0.004)	0.538 (0.005)	3.33 (0.08)	6.15 (0.26)
BD06	26/22N/32E	1.503 (0.008)	10.49 (0.04)	0.0561 (0.0004)	9197 (161)	1.20 (0.02)	0.202 (0.002)	0.350 (0.003)	1.35 (0.04)	NM
BD07	3/19N/33E	2.104 (0.011)	11.20 (0.05)	0.0542 (0.0004)	10,923 (308)	0.781 (0.010)	0.180 (0.002)	0.280 (0.003)	0.900 (0.036)	1.96 (0.10)
BD08	9/18N/33E	1.143 (0.006)	10.21 (0.03)	0.0578 (0.0004)	6643 (65)	1.61 (0.02)	0.264 (0.003)	0.396 (0.004)	2.00 (0.05)	NM
BD09	17/21N/33E	1.724 (0.009)	10.74 (0.05)	0.0578 (0.0005)	NM	0.981 (0.012)	0.180 (0.002)	NM	NM	NM
BD10	7/22N/34E	1.104 (0.006)	10.20 (0.02)	0.0537 (0.0003)	6719 (81)	1.99 (0.03)	0.308 (0.003)	0.396 (0.003)	2.02 (0.05)	NM
BD11	25/19N/30E	3.784 (0.019)	11.88 (0.05)	0.0565 (0.0004)	21,453 (1274)	0.391 (0.005)	0.103 (0.001)	0.241 (0.004)	0.455 (0.019)	9.94 (0.09)
BD12	27/19N/30E	3.627 (0.018)	NM	NM	20,888 (1017)	0.415 (0.006)	NM	0.242 (0.003)	0.467 (0.024)	NM
BD13	22/18N/35E	1.318 (0.007)	10.25 (0.05)	0.0579 (0.0005)	7714 (220)	1.53 (0.02)	0.240 (0.003)	0.382 (0.004)	1.92 (0.05)	3.18 (0.06)
BD14	16/18N/34E	1.413 (0.007)	10.54 (0.12)	0.0583 (0.0002)	8490 (523)	1.15 (0.02)	0.179 (0.004)	0.307 (0.003)	1.23 (0.04)	NM
BD12b	27/19N/30E	3.634 (0.018)	11.60 (0.06)	0.0537 (0.0002)	22,492 (2474)	0.413 (0.006)	0.120 (0.002)	0.240 (0.004)	0.490 (0.024)	NM

1σ errors quoted in brackets. $^{3}He/^{4}He$ are relative to the atmospheric ratio ($R/R_a = 1.39 \times 10^{-6}$).
NM = not measured.

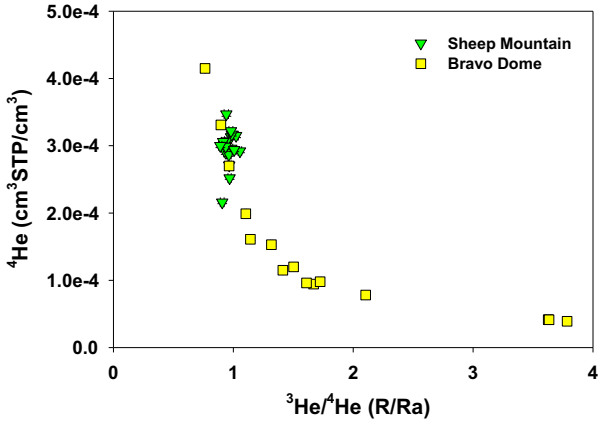

Fig. 1. Plot of ^{3}He/^{4}He (R/R$_a$) against ^{4}He concentration for the samples in this study. Bravo Dome ^{3}He/^{4}He ratios exhibit clear mixing between a high ^{3}He/^{4}He mantle end member and a low ^{3}He/^{4}He crust end member. Values within the Sheep Mountain field show minimal variation. Error bars are smaller than printed symbols.

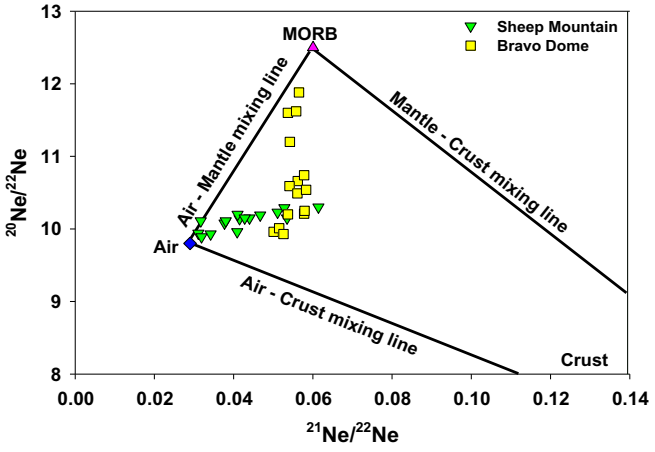

Fig. 2. Plot of ^{20}Ne/^{22}Ne ratio against ^{21}Ne/^{22}Ne for samples from Sheep Mountain and Bravo Dome. The plot highlights two distinct mixing trends; mixing between an air/crust mixture and the mantle, observed in Bravo Dome, and mixing between a mantle/crust mix and air, observed in Sheep Mountain. Error bars are smaller than printed symbols.

$$[^{40}\mathrm{Ar}]_{\mathrm{corrected}} = [^{40}\mathrm{Ar}]_{\mathrm{measured}} \times \left[1 - \frac{(^{40}\mathrm{Ar}/^{36}\mathrm{Ar})_{\mathrm{air}}}{(^{40}\mathrm{Ar}/^{36}\mathrm{Ar})_{\mathrm{measured}}}\right] \quad (1)$$

Air corrected ^{40}Ar constitutes 93.7% to 98.7% of the ^{40}Ar measured in Bravo Dome, which is comprised of both mantle and crustal contributions. Due to the correlation between crust and mantle ratios within the field, the mantle and crust contributions to ^{40}Ar can be resolved using the methods outlined in Section 5.1.

Air corrected ^{40}Ar concentrations from Sheep Mountain vary from 1.30×10^{-4} to 2.04×10^{-4} cm^3(STP)cm^{-3}, constituting 93.3% to 98.6% of the total ^{40}Ar. As there is no consistent variation in the crust and mantle ratios within the field, contributions of ^{40}Ar$_{\mathrm{mantle}}$ and ^{40}Ar$_{\mathrm{crust}}$ cannot be resolved and the air corrected ^{40}Ar must be considered in terms of ^{40}Ar$_{\mathrm{crust + mantle}}$.

5. Discussion

5.1. Resolving mantle and crust components

5.1.1. Bravo Dome

As previously outlined in Section 4.2, the distinct isotopes of Ne can be used to resolve the air, crust and mantle components from any sample. This enables the resolved ^{21}Ne$_{\mathrm{air}}$ component to be subtracted from the ^{21}Ne$_{\mathrm{total}}$, leaving 'air-corrected' ^{21}Ne$_{\mathrm{crust + mantle}}$. Plotting ^{21}Ne$_{\mathrm{crust + mantle}}$/^{4}He against ^{3}He/^{4}He (which has a negligible air component) defines a simple two-component mixing line (Fig. 3(a)). This can be extrapolated to the well-defined crustal ^{3}He/^{4}He endmember of 0.005 R$_a$ (Ballentine and Burnard, 2002) allowing the local ^{4}He/^{21}Ne$_{\mathrm{crust}}$ input value to be resolved as $3.47 \pm 0.24 \times 10^7$, when a ^{20}Ne/^{22}Ne$_{\mathrm{mantle}}$ of 12.5 is used (Ballentine et al., 2005). The estimate of the mantle Ne endmember within the Bravo Dome field has been further refined by Holland and Ballentine (2006) to be 12.49 ± 0.04 for ^{20}Ne/^{22}Ne and 0.0578 ± 0.0003 for ^{21}Ne/^{22}Ne. This confirms that use of a ^{20}Ne/^{22}Ne$_{\mathrm{mantle}}$ of 12.5 is valid for this field.

This ^{4}He/^{21}Ne$_{\mathrm{crust}}$ ratio can then be combined with the resolved ^{21}Ne$_{\mathrm{crust}}$ value to calculate the crustal contributions to ^{3}He and ^{4}He. This allows a resolved ^{3}He/^{4}He$_{\mathrm{mantle}}$ value to be calculated for each sample. The ^{3}He/^{4}He$_{\mathrm{mantle}}$ determined in three samples have propagated errors which are < 50% and these provide an error-weighted average of 5.35 ± 0.36 to 7.4 ± 0.5 R$_a$ for the ^{3}He/^{4}He$_{\mathrm{mantle}}$ end member as outlined in detail in Ballentine et al. (2005). We determine a corresponding range of ^{4}He/^{21}Ne*$_{\mathrm{mantle}}$ values by combining the resolved ^{4}He$_{\mathrm{mantle}}$ values with those of ^{21}Ne*$_{\mathrm{mantle}}$. This ^{21}Ne*$_{\mathrm{mantle}}$ value is calculated using the neon 3-isotope technique outlined in Section 4.2 and then performing a correction for the solar contributions using the method outlined by Graham (2002).

A plot of ^{40}Ar$_{\mathrm{crust + mantle}}$/^{4}He plotted against ^{3}He/^{4}He also generates a two component mixing line allowing the ^{4}He/^{40}Ar$_{\mathrm{crust}}$ input value to be determined (Fig. 3(b)). Extrapolation to the ^{3}He/^{4}He$_{\mathrm{mantle}}$

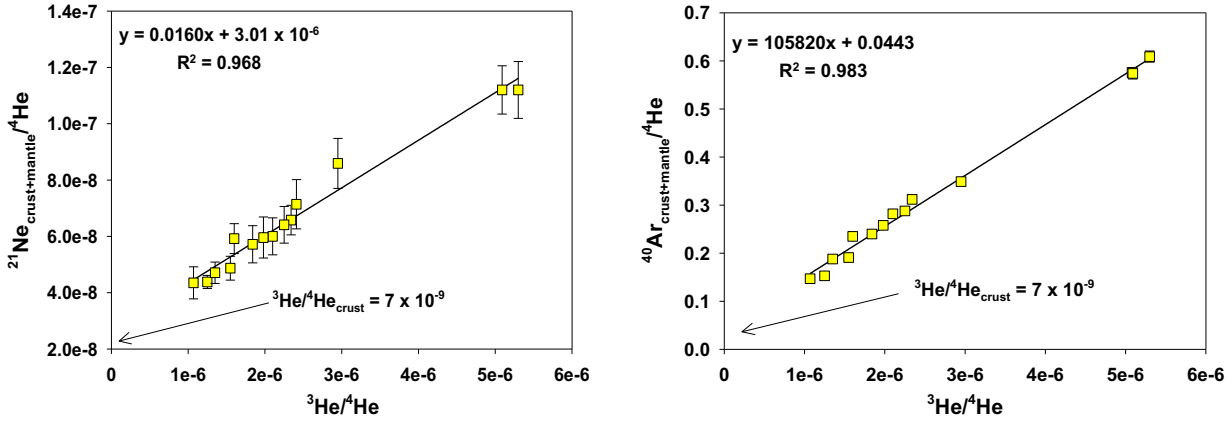

Fig. 3. (a) Left. Resolving crust and mantle end members using simple mixing. Elemental Ne/He (a) and Ar/He (b) ratios plotted against ^{3}He/^{4}He for samples from Bravo Dome exhibit simple mantle-crust two component mixing lines. Extrapolation to the crustal ^{3}He/^{4}He end member value allows the crustal input ratio to the field to be determined as 7×10^9. The lack of variation in the ^{3}He/^{4}He ratio in the Sheep Mountain field (Fig. 1) prevents this technique being used the resolve the crustal contribution to the field.
Figures reproduced from Ballentine et al. (2005).

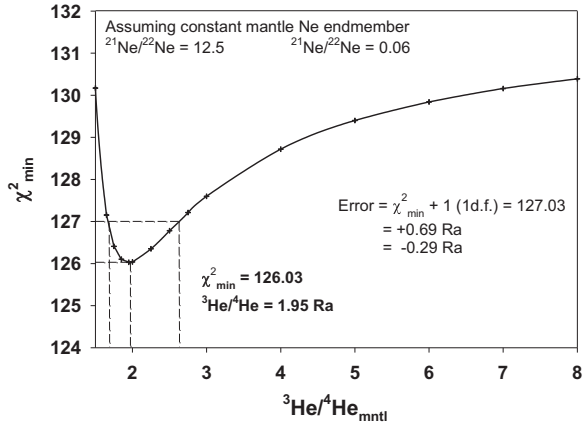

Fig. 4. χ^2 minimisation on the variance of resolved $^4He/^{21}Ne_{crust}$ values as a function of $^3He/^4He_{mantle}$ end member. The χ^2_{min}/ν = 9.00 for 14 degrees of freedom, suggesting a poor minimisation. The variance in the $^4He/^{21}Ne_{crust}$ values minimises to a $^3He/^4He_{mantle}$ ratio of 1.95 R_a. However, the 1 δ error bars defined by χ^2_{min} + 1 produces a wide range of potential $^3He/^4He$ values of 1.66 to 2.64 R_a.

value determined above provides the range of resolved $^{40}Ar/^4He_{mantle}$ and allows mantle and crust contributions to be corrected from the air corrected $^{40}Ar_{crust\ +\ mantle}$ as outlined in Ballentine et al. (2005).

5.1.2. Sheep Mountain

The variation of $^3He/^4He$ in the Sheep Mountain field is insufficient to allow extrapolation to the crustal $^3He/^4He$ end member and therefore the techniques outlined for Bravo Dome by Ballentine et al. (2005) cannot be applied in this instance. This means that the crustal input values in the field cannot be determined directly. However, we have developed a method to constrain the range of mantle $^3He/^4He$, $^4He/^{21}Ne^*$, $^3He/^{22}Ne$, $^4He/^{40}Ar$ and $^{21}Ne^*/^{40}Ar$ values within the dataset using chi-squared minimisation techniques.

The technique uses the $^{21}Ne_{crust}$ abundance calculated from the air, crust and mantle Ne end members. Assuming a MORB-like mantle source of 8 R_a for the well gases allows the resolved MORB $^{20}Ne/^{22}Ne_{mantle}$ and $^{21}Ne/^{22}Ne_{mantle}$ values of 12.5 value and 0.06 to be used (Ballentine et al., 2002; Ballentine et al., 2005; Holland and Ballentine, 2006). Note that three samples that are closet to the air end member are not used (2-9-H, 1-15-C and 5-15-O), as the crust and mantle components cannot be resolved in these samples, due to the presence of a large air-derived component from the formation water.

The range exhibited of $^4He/^{20}Ne$ from Sheep Mountain samples of 3200 to 71,100 is significantly above the air ratio value of 0.32 (Kipfer et al., 2002). Therefore, the $^3He/^4He$ ratio can be considered as a sum of only two components, the crust and the mantle. The contribution of ^4He from the crust can be calculated for different $^3He/^4He_{mantle}$ ratios using the following formula (Ballentine et al., 2002);

$$[^4He]_{crust} = [^4He]_{tot} \times \frac{\left[\frac{^3He}{^4He}\right]_{mntl} - \left[\frac{^3He}{^4He}\right]_{meas}}{\left[\frac{^3He}{^4He}\right]_{mntl} - \left[\frac{^3He}{^4He}\right]_{crust}} \quad (2)$$

As the $^4He_{crust}$ is dependent on the $^3He/^4He_{mantle}$ end member, so too is the $^4He/^{21}Ne_{crust}$ ratio as $^{21}Ne_{crust}$ is derived independently from the He system. Hence, for each sample, $^4He/^{21}Ne_{crust}$ values can be determined as the $^3He/^4He_{mantle}$ is varied from 1 to 8 R_a. For each $^3He/^4He_{mantle}$ ratio used an error-weighted mean $^4He/^{21}Ne_{crust}$ ($\bar{x}$) using Eq. (3), and the associated weighted uncertainty Eq. (4) can be calculated from the dataset as follows:

$$\bar{x} = \frac{\sum_{i=1}^{n} x_i/\sigma_i^2}{\sum_{i=1}^{n} 1/\sigma_i^2} \quad (3)$$

$$\sigma_{\bar{x}} = \sqrt{\frac{1}{\sum_{i=1}^{n} 1/\sigma_i^2}} \quad (4)$$

where:

σ_i is the uncertainty attributed to each sample.

Variable correction on each sample for the mantle component will leave differing crustal $^4He/^{21}Ne_{crust}$ residues. If we make the assumption that the field has been subjected to a constant crustal $^4He/^{21}Ne_{crust}$ input, as evidenced by the low variance of $^3He/^4He$ observed, then we would expect the 'correct' mantle $^3He/^4He$ value to exhibit the least deviation of the residual $^4He/^{21}Ne_{crust}$ from the error weighted mean value. We can then determine the 'best fit' mantle $^3He/^4He_{mantle}$ end member using a Reduced Chi-Squared minimisation (x^2_{min}), with confidence limits on this determination providing an assessment of the statistical significance of the fit.

$$x^2_{min} = \sum \frac{(O_i - \bar{x})^2}{\sigma_i^2} \quad (5)$$

where O_i = individual observed calculated $^4He/^{21}Ne_{crust}$ ratio for each sample.

Fig. 4 shows the Reduced Chi-Squared minimisation for the $^3He/^4He_{mantle}$ range of 1 to 8 R_a. Whilst the dataset exhibits a minimisation at 1.95 R_a, the 1σ confidence limits defined by χ^2_{min} + 1 produces a range of possible $^3He/^4He$ values of 1.66 to 2.64 R_a. The wide range of derived $^3He/^4He_{mantle}$ and high Chi-Squared value of 9 (for 14 degrees of freedom) implies there could be another variable in the dataset that is not accounted for in this simple minimisation.

As the resolved $^3He/^4He_{mantle}$ is significantly below that of MORB, using the mantle Ne end members corresponding to an 8 R_a mantle source may be inappropriate. As previously highlighted many He isotope studies have identified that the isotopic ratio of He within the SCLM is more radiogenic than that of the mid ocean ridge (MORB) source mantle. Gautheron et al. (2005) report a homogenous $^3He/^4He_{mantle}$ for the European SCLM of 6.32 ± 0.39 R_a that they attribute to two potential mechanisms that allow asthenospheric helium to invade the lithosphere: recent, local metasomatism or global, continuous metasomatism in a steady state for helium. This work also inferred that the Ne systematics of the SCLM beneath Europe is also more radiogenic than that of MORB. Recent work by Bräuer et al. (2013) has reported a SCLM Ne composition in the Eifel area that represents mixing of a MORB-like Ne component with a fractionated atmospheric component, but also shows evidence of the presence of a small radiogenic Ne component in a number of samples.

Radiogenic ingrowth in the mantle source could also account for the low $^3He/^4He_{mantle}$ resolved in the Sheep Mountain reservoir. In order to test this theory, we model the increase in $^{21}Ne/^{22}Ne$ that will result from radiogenic production of ^{21}Ne, which will be proportional to the amount of ^4He required to reduce the $^3He/^4He_{mantle}$ from 8 R_a to 2 R_a. This can be achieved as the ^3He concentration of the convecting mantle is known, from a combination of the ^3He flux from mid ocean ridges (Craig et al., 1975) and MORB popping rock measurements, to be 4.4×10^{-11} cm^3 STP g^{-1} (Moreira et al., 1998), assuming 10% partial melting (Porcelli and Ballentine, 2002).

Hence, using the MORB $^3He/^4He$ of 8 R_a, the ^4He concentration of the convecting mantle can be calculated as 3.93×10^{-6} cm^3 STP g^{-1}. Combining this with the measured $^4He/^{21}Ne^*$ value of MORB of 1.68×10^7 (Moreira et al., 1998) gives a $^{21}Ne^*$ concentration of 2.34×10^{-13} cm^3 STP g^{-1}. Using these values, the amount of ^4He required to reduce the $^3He/^4He_{mantle}$ ratio by radiogenic ingrowth from 8 R_a to 2 R_a can be calculated to be 1.57×10^{-5} cm^3 STP g^{-1}.

This can be combined with estimates of the present day $^4He/^{21}Ne^*$ production rates in the mantle which vary between 2.22×10^7 (Yatsevich and Honda, 1997) and 2.79×10^7 (Leya and Wieler, 1999) to determine the amount of ^{21}Ne produced. This is directly proportional

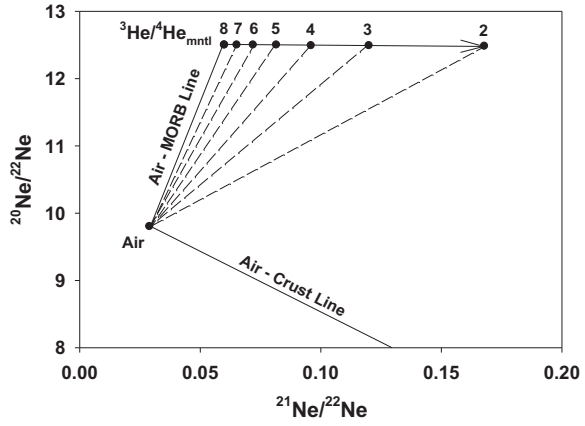

Fig. 5. Plot of the $^{20}Ne/^{22}Ne$ against $^{21}Ne/^{22}Ne$ showing the effect of mantle radiogenic addition on the $^{21}Ne/^{22}Ne_{mantle}$ ratio correlated with a reduction of the $^{3}He/^{4}He_{mantle}$ ratio from 8 to 2 R_a. Note that this is dependent on the mantle $^{4}He/^{21}Ne$ production ratio used and is independent of any assumed mantle ^{4}He concentration.

to the quantity of radiogenic ^{4}He excess required to lower the $^{3}He/^{4}He_{mantle}$ to the resolved value. Adding this to the original ^{21}Ne concentration of the mantle, allows the $^{21}Ne/^{22}Ne_{mantle}$ corresponding to the lower $^{3}He/^{4}He_{mantle}$ to be calculated (Fig. 5). We use estimates of mantle noble gas concentrations derived from popping rock, which have been recently cited to be above other estimates (Bianchi et al., 2010). However, it should be noted that the increase in the $^{21}Ne/^{22}Ne$ ratio corresponding to the reduction in $^{3}He/^{4}He_{mantle}$ is solely dependent on the $^{4}He/^{21}Ne^{*}$ mantle production ratio used and is therefore independent of absolute concentrations.

Using the same method as previously outlined we now perform a Reduced Chi-Squared minimisation for lower $^{3}He/^{4}He_{mantle}$ values, but now couple it with the corresponding increase in the mantle $^{21}Ne/^{22}Ne$ end member. We perform this minimisation for both of the current estimates of $^{4}He/^{21}Ne_{mantle}$ production. These two separate minimisations produce much lower χ^2_{min} values of 2.13 for a $^{4}He/^{21}Ne^{*}$ of 2.22×10^7 and 2.12 for a $^{4}He/^{21}Ne^{*}$ of 2.79×10^7, for 14 degrees of freedom, indicating a more statistically significant resolution of the $^{3}He/^{4}He_{mantle}$ value.

This highlights that radiogenic production within the SCLM source which supplies volatiles to the field, could be responsible for reducing both the $^{3}He/^{4}He_{mantle}$ and a corresponding increase in the $^{21}Ne/^{22}Ne_{mantle}$ end member. The two minimisations give a range of values for $^{3}He/^{4}He_{mantle}$ of 2.59 ± 0.15 to 3.00 ± 0.18, and a corresponding range of weighted mean $^{4}He/^{21}Ne_{crust}$ values of 2.86 ± 0.30 and 3.08 ± 0.32 × 10^7, respectively (Fig. 6(a) & (b)). Confidence in this procedure is reinforced by the fact that resolved $^{4}He/^{21}Ne_{crust}$ values are similar to those measured in Bravo Dome of 3.47 ± 0.24 × 10^7 (Ballentine et al., 2005).

Using the derived range of $^{3}He/^{4}He_{mantle}$ values, a similar Reduced Chi-Squared minimisation can be performed to constrain the $^{4}He/^{40}Ar_{mantle}$ of the Sheep Mountain field. The $^{40}Ar_{mantle}$ contribution can then be simply determined through multiplication of the previously calculated $^{4}He_{mantle}$ concentration by the resolved $^{4}He/^{40}Ar_{mantle}$ ratio. This in turn permits the $^{40}Ar_{crust}$ to be determined through subtraction of the calculated $^{40}Ar_{mantle}$ contribution from the $^{40}Ar_{crust\ +\ mantle}$ value. The independently calculated $^{21}Ne_{crust}$ value obtained independently from the Ne three isotope method can then be combined with the $^{40}Ar_{crust}$ to provide the $^{21}Ne/^{40}Ar_{crust}$ of each sample.

Therefore, for each sample, $^{21}Ne/^{40}Ar_{crust}$ values can be determined as the $^{4}He/^{40}Ar_{mantle}$ is changed. This allows an error-weighted mean $^{21}Ne/^{40}Ar_{crust}$ to be calculated from the dataset. If we assume that the field has been subjected to a constant crustal $^{21}Ne/^{40}Ar_{crust}$ input, similar to the assumption made for $^{4}He/^{21}Ne_{crust}$, then the 'correct' mantle $^{4}He/^{40}Ar_{mntl}$ end member should result in the least deviation in

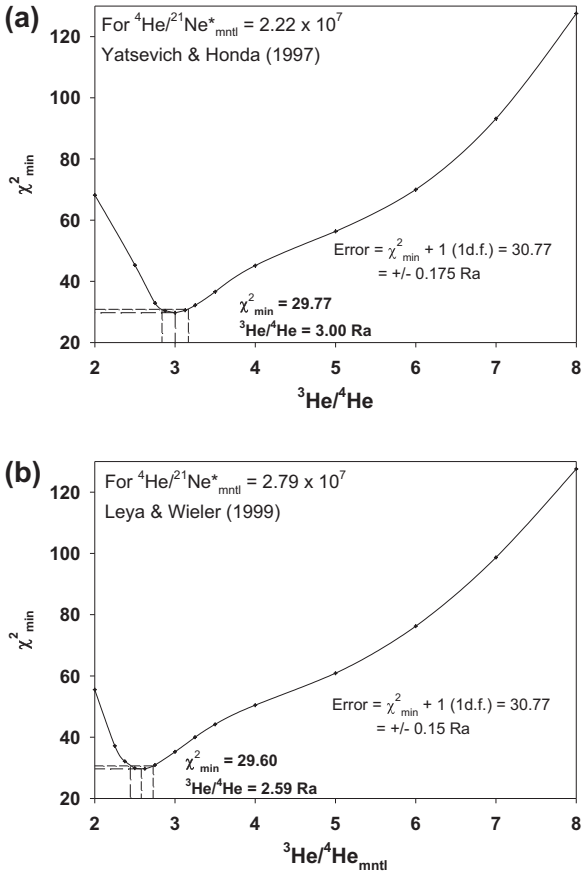

Fig. 6. (a). χ^2 minimisation on the variance of resolved $^{4}He/^{21}Ne_{crust}$ values as a function of $^{3}He/^{4}He_{mantle}$ end member and corresponding increase in $^{21}Ne/^{22}Ne$ using a $^{4}He/^{21}Ne^{*}_{mantle}$ ratio of 2.22 × 10^7. The χ^2_{min}/ν = 2.12 for 14 degrees of freedom. The variance of $^{4}He/^{21}Ne_{crust}$ minimises to a $^{3}He/^{4}He_{mantle}$ ratio of 3.00 R_a. For 1 degree of freedom the 68.3% confidence limit is determined by the χ^2_{min} value + 1. This gives a range of $^{3}He/^{4}He_{mantle}$ of 3.00 ± 0.18 R_a corresponding to a resolved $^{4}He/^{21}Ne_{crust}$ value of 3.08 ± 0.32.
(b). χ^2 minimisation on the variance of resolved $^{4}He/^{21}Ne_{crust}$ values as a function of $^{3}He/^{4}He_{mantle}$ end member and corresponding increase in $^{21}Ne/^{22}Ne$ using a $^{4}He/^{21}Ne^{*}_{mantle}$ ratio of 2.79 × 10^7. The χ^2_{min}/ν = 2.12 for 14 degrees of freedom. The variance of $^{4}He/^{21}Ne_{crust}$ minimises to a $^{3}He/^{4}He_{mantle}$ ratio of 2.59 R_a ± 0.15 R_a corresponding to a resolved $^{4}He/^{21}Ne_{crust}$ value of 2.90 ± 0.30.

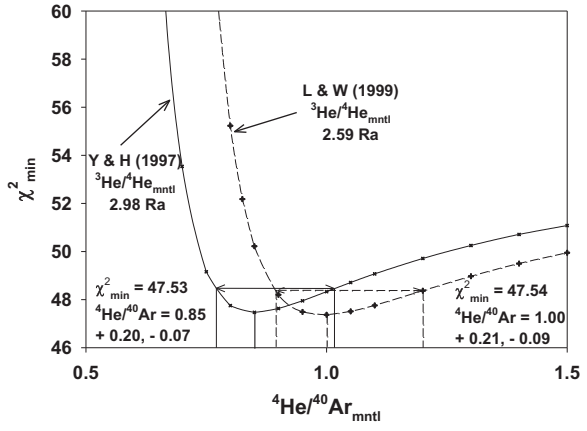

Fig. 7. χ^2 minimisation on the variance of resolved $^{21}Ne/^{40}Ar_{crust}$ values as a function of $^{4}He/^{40}Ar_{mantle}$ end member. The χ^2_{min}/ν = 3.40 for 14 degrees of freedom. The variance of $^{21}Ne/^{40}Ar_{crust}$ minimises to a $^{4}He/^{40}Ar_{mantle}$ ratio of 1.00, + 0.21, − 0.09 for a $^{3}He/^{4}He_{mantle}$ ratio of 2.59 R_a (dashed line), and to a ratio of 0.85, + 0.20, − 0.07 for a $^{3}He/^{4}He_{mantle}$ of 3.00 R_a (solid line).

Table 2
Resolved mantle elemental and isotopic ratios.

Source	$^{3}He/^{4}He_{mantle}$ (R_a)	$^{4}He/^{21}Ne^{*}_{mantle}$ ($\times 10^{7}$)	$^{3}He/^{22}Ne_{mantle}$	$^{4}He/^{40}Ar_{mantle}$	$^{21}Ne/^{40}Ar_{mantle}$ ($\times 10^{-8}$)
Popping rock	8.22 ± 0.15*	1.68	4.90	1.52	6.31
(Moreira et al., 1998; *Burnard et al., 1997)	8.54 ± 0.12				9.05
Bravo Dome	5.35 ± 0.36	1.45	2.77	0.844	5.82
(Ballentine et al., 2005; 'Holland and Ballentine, 2006)	7.40 ± 0.50'	1.23'	2.56'	1.09'	8.86'
Sheep Mountain	2.59 ± 0.15	1.30 ± 0.14	2.80 ± 0.16	1.00 + 0.21, − 0.09	7.70 ± 1.54
	3.00 ± 0.18	1.11 ± 0.11	2.80 ± 0.16	0.85 + 0.20, − 0.07	7.66 ± 1.62

$^{21}Ne^{*}$ indicates ^{21}Ne corrected for solar contribution (Graham, 2002).

$^{21}Ne/^{40}Ar_{crust}$ values from the error-weighted mean. This minimisation is shown in Fig. 7 and enables us to derive a $^{4}He/^{40}Ar_{mantle}$ range of 0.85 (+0.20, −0.07) to 1.00 (+0.21, −0.09). Multiplication of the inverse of the $^{4}He/^{21}Ne_{mantle}$ range with the $^{4}He/^{40}Ar_{mantle}$ values allows the range of $^{21}Ne/^{40}Ar_{mantle}$ values to be derived. All of the resolved mantle ratio ranges are documented in Table 2.

5.2. Resolved mantle components

We now consider the resolved mantle ratios, specifically $^{3}He/^{22}Ne_{mantle}$, $^{4}He/^{21}Ne^{*}_{mantle}$, $^{4}He/^{40}Ar_{mantle}$ and $^{21}Ne/^{40}Ar_{mantle}$.

5.2.1. $^{3}He/^{4}He_{mantle}$ and $^{3}He/^{22}Ne_{mantle}$ ratios

We first investigate the relationship between $^{3}He/^{4}He_{mantle}$ and the elemental $^{3}He/^{22}Ne_{mantle}$. As neither isotope is significantly produced by radiogenic mechanisms, the measured ratio should be unaffected by the radiogenic lowering of the $^{3}He/^{4}He_{mantle}$ within the gas fields. It is therefore significant that the resolved range of $^{3}He/^{22}Ne_{mantle}$ in both fields is lower than that of MORB (Fig. 8). This implies that there is a process in addition to radiogenic ingrowth that is fractionating the $^{3}He/^{22}Ne_{mantle}$ in both settings.

In the Bravo Dome field, values vary from 2.56 to 2.77, 1.8–1.9 times lower than the measured MORB popping rock value of 4.90 (Burnard et al., 1997; Moreira et al., 1998). Importantly, the small range of resolved $^{3}He/^{22}Ne_{mantle}$ in Sheep Mountain of 2.80–2.81 ± 0.16 is indistinguishable from the range of values resolved in Bravo Dome, some 1.75 times lower than the MORB value. This shows that the Sheep Mountain field, after correction for radiogenic production in the mantle through use of a higher $^{21}Ne/^{22}Ne$ end member, has an identical elemental $^{3}He/^{22}Ne_{mantle}$ to that of Bravo Dome. This implies that a similar process could be responsible for lowering the $^{3}He/^{22}Ne_{mantle}$ in both fields. These values are similar to the ratio of 1.91 previously resolved from a comprehensive suite of well gases (Ballentine et al., 1997).

Tucker and Mukhopadhyay (2014) have recently reported

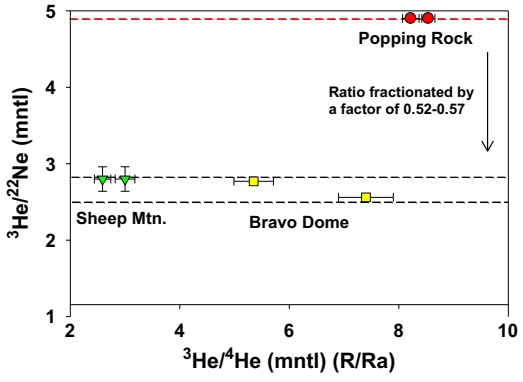

Fig. 8. Plot of the resolved elemental $^{3}He/^{22}Ne_{mantle}$ against the corresponding mantle $^{3}He/^{4}He_{mantle}$ for the two gas fields. Both Bravo Dome and Sheep Mountain exhibit a similar reduction (factor of 0.52–0.57) in $^{3}He/^{22}Ne_{mantle}$ ratios compared to the values observed in MORB.

equatorial Atlantic MORBs derived from a heterogeneous source with $^{3}He/^{22}Ne_{mantle}$ ratios of 6.1 to 9.8. They observed that the most depleted MORBs are derived from a mantle with the highest $^{3}He/^{22}Ne_{mantle}$ ratios, whilst more enriched MORBs corresponded to lower $^{3}He/^{22}Ne_{mantle}$ values. Average $^{3}He/^{22}Ne_{mantle}$ ratios of 10.2 ± 1.6 were reported by (Honda and McDougall, 1998) from 20 measurements and a value of 8.8 ± 3.5 was compiled by (Graham, 2002) from an average of 85 measurements. Jalowitzki et al. (2016) report higher than depleted MORB $^{3}He/^{22}Ne$ ratios for the local SCLM endmember beneath Southern Patagonia of 12.03 ± 0.15 to 13.66 ± 0.37.

However, direct measurements of $^{3}He/^{22}Ne$ ratios in mantle-derived basalts are not believed to represent the mantle value as the ratio can be readily changed by magmatic degassing during eruption and ubiquitous shallow-level air contamination (Tucker and Mukhopadhyay, 2014). Therefore, the ranges cited above were calculated from combining measured He and Ne isotope ratios in basalts, after the methods outlined by Honda and McDougall (1998) and Porcelli and Ballentine (2002). Further, the values reported by Graham (2002) and Honda and McDougall (1998) were calculated assuming a mantle $^{20}Ne/^{22}Ne$ ratio of 13.8.

The average $^{3}He/^{22}Ne_{mantle}$ ratios of Honda and McDougall (1998) and Graham (2002) recalculated using $a^{20}Ne/^{22}Ne = 12.5$ are 7.3 ± 1.2 and 6.1 ± 2.4, respectively (Tucker and Mukhopadhyay, 2014), close to, or within, the MORB popping rock value of 4.9 that we use. Further, a higher MORB $^{3}He/^{22}Ne_{mantle}$ ratio makes our dataset more difficult to explain and hence we use what we believe to be the most accurate unfractionated value. The higher $^{3}He/^{22}Ne$ ratios recently reported from Southern Patagonia are believed to indicate that the SCLM here experienced a different evolution from a MORB source than other SCLMs (Jalowitzki et al., 2016). These higher ratios were attributed to greater compatibility of He relative to Ne during melt extraction linked to a vertical delamination process related to subduction in the area and hence are not directly relevant to our observations.

5.2.2. Equilibrium partitioning

Previous studies have shown that equilibrium partitioning of He and Ne between a melt and gas phase can decrease the He/Ne ratio in the gas phase (Jambon et al., 1986; Lux, 1987). The magnitude of this fractionation, $F[He/Ne]_{gas}$, is defined by the He/Ne ratio in the gas phase, $[He/Ne]_{gas}$, divided by the original He/Ne ratio in the melt, $[He/Ne]_{melt}$, prior to the formation of the gas phase. Equilibrium partitioning between He and Ne can be modelled using their respective Henry's solubility constants. The absolute solubilities of noble gases in a silicate melt are only weakly affected by temperature and therefore are typically calculated as a function of the percentage ionic porosity (Carroll and Draper, 1994). When the gas/melt volume ratio approaches zero, He and Ne in the gas phase are fractionated proportionally to their relative solubilities in the melt and $F(He/Ne)_{gas}$ reaches a maximum (where $F[He/Ne]_{gas} \rightarrow K_{Ne}/K_{He}$ when K_{He} and K_{Ne} are the respective Henry coefficients for He and Ne). Fig. 9 shows the maximum $F[He/Ne]_{gas}$ against percent ionic porosities of 45–52%.

Assuming initial MORB mantle values of 4.9 for $^{3}He/^{22}Ne_{mantle}$ as explained above, the fractionation factor ($F[He/Ne]$) required to

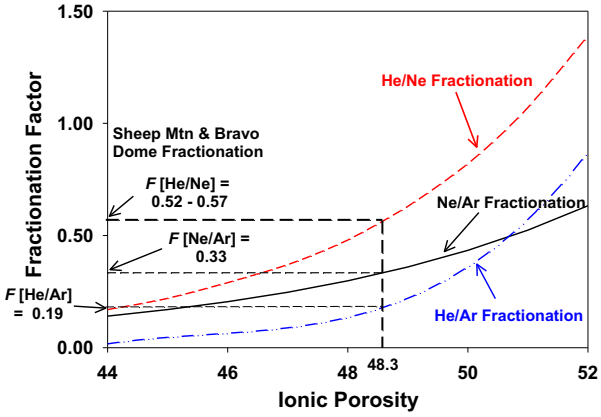

Fig. 9. Plot of the fractionation factor against % melt ionic porosity for He/Ne, Ne/Ar and He/Ar. Maximum fractionation occurs in the gas phase as the gas/melt volume approaches zero. Data from Carroll and Draper (1994) are used. For He/Ne a maximum melt ionic porosity of 48.3% is required to account for the fractionation observed in both Sheep Mountain and Bravo Dome.

account for the $^{3}He/^{22}Ne_{mantle}$ of 2.80 measured in the Sheep Mountain field is ~0.57, almost identical to the *F*[He/Ne] range of 0.52 to 0.56 required to account for the Bravo Dome range of 2.56–2.77. These fractionation factors can be accounted for by ionic porosity in the degassing melt of ~48.3% for both datasets (Fig. 9). Ionic porosity is crudely anti-correlated to melt density and a melt density of 2.6 g cm^{-3}, can account for the derived ionic porosity, provided that the gas/melt ratio is small. Higher ionic porosities and lower melt densities than these cannot account for the minimum fractionation observed within the fields. These values are comparable with the lower end of the density range of typical mafic melts (10–20% partial melt) of 2.6–2.7 g cm^{-3} (Ballentine, 1997).

5.2.3. $^{3}He/^{4}He_{mantle}$ and $^{4}He/^{21}Ne^{*}_{mantle}$ ratios

As radiogenic ingrowth of ^{4}He can account for the reduction of the Sheep Mountain $^{3}He/^{4}He_{mantle}$, it is straightforward to calculate the amount of ^{4}He required to lower the values measured in the field. Using the calculated mantle production ratio range for $^{4}He/^{21}Ne^{*}$ of 2.22×10^{7} (Leya and Wieler, 1999) and 2.79×10^{7} (Yatsevich and Honda, 1997) enables the amount of ^{21}Ne corresponding to this ^{4}He excess to also be calculated. This allows a range of predicted $^{4}He/^{21}Ne^{*}_{mantle}$ ratios that correspond to the $^{3}He/^{4}He_{mantle}$ reduction to be determined. In the Bravo Dome field the highest $^{3}He/^{4}He_{mantle}$ value measured of 7.40 R_a is extremely close to that of MORB and therefore radiogenic production should not significantly alter the $^{4}He/^{21}Ne^{*}_{mantle}$. Applying the same methodology to the Sheep Mountain field, the reduction of the $^{3}He/^{4}He_{mantle}$ to between 2.59 and 3.00 R_a would result in an increase of the $^{4}He/^{21}Ne^{*}_{mantle}$ to between 2.01 and 2.30×10^{7} and 1.98–2.24×10^{7}, respectively (Fig. 9).

However, the actual $^{4}He/^{21}Ne^{*}_{mantle}$ range resolved in the Bravo Dome field of 1.23–1.45×10^{7} is between 1.2 and 1.4 times lower than the measured MORB popping rock value. $^{4}He/^{21}Ne^{*}_{mantle}$ resolved in the Sheep Mountain field range from 1.11 ± 0.11 to $1.30 \pm 0.14 \times 10^{7}$, between 1.3 and 1.5 times lower than the MORB value and only slightly below the Bravo Dome value (Fig. 10). This reduction could be explained by the same phase partitioning process outlined to account for the reduction in $^{3}He/^{22}Ne_{mantle}$. Applying the same maximum fractionation factor of 0.52 observed in the $^{3}He/^{22}Ne_{mantle}$ produces two fractionation lines that can account for one of the set of values measured in Sheep Mountain (Fig. 10). The resolved range from the other Sheep Mountain value and from Bravo Dome, are however, somewhat above the predicted line, implying that fractionation of the $^{4}He/^{21}Ne^{*}_{mantle}$ has not been as severe as that observed in the $^{3}He/^{22}Ne_{mantle}$ within the field.

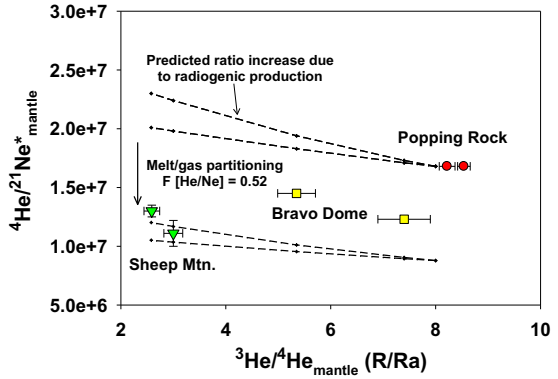

Fig. 10. Plot of the resolved radiogenic $^{4}He/^{21}Ne^{*}_{mantle}$ against the corresponding mantle $^{3}He/^{4}He_{mantle}$ for Bravo Dome and Sheep Mountain. Also shown is the predicted ratio increase which would result from radiogenic production of ^{4}He and ^{21}Ne in the mantle, and how these ratios would be reduced by the same degree of phase partitioning as the maximum observed in the $^{3}He/^{22}Ne_{mantle}$ ratios ($F = 0.52$). Whilst one of the Sheep Mountain values can be accounted for by this model it is obvious that the $^{4}He/^{21}Ne_{mantle}$ fractionation has been less severe than that of $^{3}He/^{22}Ne_{mantle}$.

5.2.4. $^{3}He/^{4}He_{mantle}$, $^{4}He/^{40}Ar_{mantle}$ and $^{21}Ne/^{40}Ar_{mantle}$

The radiogenic production ratio of $^{4}He/^{40}Ar_{mantle}$ is ~3 (Ballentine and Burnard, 2002). Using this value with the calculated ^{4}He concentration corresponding to the individual field $^{3}He/^{4}He_{mantle}$ and the MORB value allows us to predict the increase of the $^{4}He/^{40}Ar_{mantle}$ values that would result from radiogenic production in the mantle (Fig. 11). It can be clearly seen that the $^{4}He/^{40}Ar_{mantle}$ ratios measured in both fields are considerably lower than both MORB and the predicted $^{4}He/^{40}Ar_{mantle}$ fractionation trend, implying that radiogenic production alone cannot account for the Bravo Dome and Sheep Mountain values.

However, as previously outlined, phase fractionation between a gas and melt can account for the lower He/Ne ratios measured in both fields. It is therefore probable that a similar process could be responsible for the reduction of the He/Ar ratios. As Ar is considerably less soluble in a melt than Ne, it is more readily degassed from the melt, resulting in a higher degree of fractionation within the He/Ar ratios of the exsolved gas (Carroll and Draper, 1994). This results in a high *F* [He/Ar] value of 0.19 as opposed to the *F*[He/Ne] value of 0.52 for a melt with an ionic porosity of 48.3% (Fig. 9). However, this degree of fractionation is too severe to account for the $^{4}He/^{40}Ar_{mantle}$ resolved in both gas fields (Fig. 11). This implies that there is an additional fractionation process acting on the noble gases within the field.

The model outlined by Gilfillan et al. (2008) could provide an additional process to account for the fractionation observed in the fields.

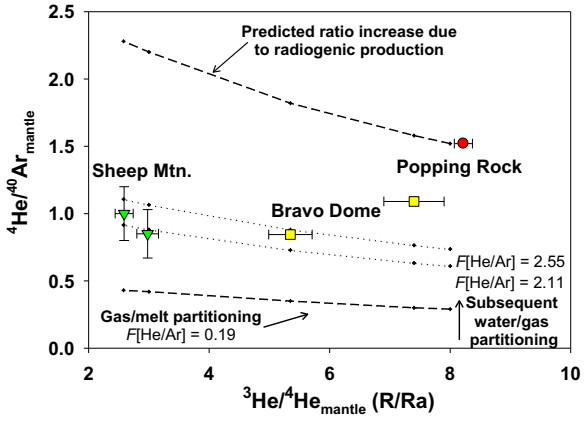

Fig. 11. Plot of the resolved $^{3}He/^{4}He_{mantle}$ ratio against the corresponding $^{4}He/^{40}Ar_{mantle}$ range. The $^{3}He/^{4}He_{mantle}$ and $^{4}He/^{40}Ar_{mantle}$ values from both fields can be explained by radiogenic ingrowth in the mantle source combined with gas/melt phase partitioning and subsequent water/gas partitioning.

In this model magmatic degassing emplaces mantle derived CO_2 and noble gases into the formation water in the gas fields. Both are subsequently degassed from the formation water upon reaching the gas/water contact. This degassing process will result in an increase in the He/Ar ratios, as He is less soluble than Ar in water, and is therefore preferentially degassed from the formation water. For the conditions in the Sheep Mountain field, the predicted *F*[He/Ar] for this process is 2.11 and within for Bravo Dome the predicted *F*[He/Ar] is 2.55. The trends that would result from this fractionation are also plotted on Fig. 11 and importantly they can account for the range of $^{4}He/^{40}Ar_{mantle}$ values observed in both fields.

Given that this process can account for the He/Ar ratios in both fields, the effect of the degassing process on the He/Ne ratios must also be considered. As the solubility of He and Ne in water is extremely similar (Crovetto et al., 1982) the *F*[He/Ne] under the reservoir conditions in Sheep Mountain and Bravo Dome will be 1.05 and 1.09, respectively, and therefore the groundwater degassing process will not significantly alter the resolved He/Ne_{mantle} in the fields.

Importantly, using exactly the same model, the resolved range of $^{21}Ne/^{40}Ar_{mantle}$ values from Sheep Mountain and the lower value from Bravo Dome can be accounted for. However, the upper values resolved in Bravo Dome for both the $^{4}He/^{40}Ar_{mantle}$ and $^{21}Ne/^{40}Ar_{mantle}$ ratios are less fractionated compared with the popping rock value than this model predicts. This corresponds to the high $^{3}He/^{4}He_{mantle}$ value of 7.40 ± 0.50 that is within the lower range of MORB, suggesting that the He/Ar and Ne/Ar ratios of the mantle rich portion of the Bravo Dome field are not significantly fractionated from MORB. At the moment it is unclear as to why the resolved $^{3}He/^{22}Ne_{mantle}$ in this portion of the field are significantly lower than MORB, whilst these values are not.

5.3. Implications to models of SCLM evolution

5.3.1. Mantle plume model

It has been suggested that a mantle plume could be the primary cause of the Cenozoic volcanism and associated high heat flow in the southwest US (Fitton et al., 1991). Several workers have also proposed that the Colorado Plateau Uplift event could be explained by the presence of a mantle plume (Parsons and McCarthy, 1995; Wilson, 1973). This has been strongly argued against by Dodson et al. (1998) and we support this argument. There is no evidence of a primitive high $^{3}He/^{4}He_{mantle}$ component within our data such as that observed in Yellowstone or Hawaii, and in fact, our derived $^{3}He/^{4}He_{mantle}$ values from the Sheep Mountain field are significantly more radiogenic than those of MORB. This is reinforced by more radiogenic than the MORB range $^{3}He/^{4}He$ measured from SCLM in extensional regions around the world including Europe (Bräuer et al., 2016; Bräuer et al., 2013; Dunai and Baur, 1995; Dunai and Porcelli, 2002; Gautheron and Moreira, 2002; Gautheron et al., 2005), the continental Cameroon Line (Barford et al., 1999), the East African Rift and in Canada (Day et al., 2005).

5.3.2. Closed system evolution of MORB mantle

Our results highlight that closed system radiogenic production can account for the low $^{3}He/^{4}He_{mantle}$ resolved from the Sheep Mountain field. Closed system radiogenic ingrowth models for the south-western US have been previously proposed by both Reid and Graham (1996) and Dodson et al. (1998). Reid and Graham concluded that the lithospheric mantle in the region is not a highly degassed reservoir contaminated by He derived from the asthenosphere. They argued that it is a reservoir which has a slightly elevated (U + Th)/^{3}He ratio (and therefore lower $^{3}He/^{4}He$) compared to the depleted upper mantle source, which has remained unmodified for 1.7 Ga. The $^{3}He/^{4}He_{mantle}$ range resolved in our Sheep Mountain sample suite of 2.59–3.00 R_a can be explained by radiogenic production of between 6.55 and 8.26×10^{-6} cm^3 STP g^{-1} of ^{4}He, assuming an initial mantle ratio of 8 R_a and a $^{4}He_{mantle}$ concentration of 3.93×10^{-6} based on the mantle ^{3}He concentration of 4.40×10^{-11} resolved by Holland et al., (2006). Using the present day mantle ^{4}He production ratio of 4.13×10^{-15} cm^3 STP g^{-1} per year (Ballentine and Burnard, 2002) requires that the upper mantle source has been isolated for a period of 1.59–1.99 Ga, comparing favourably with the value derived by Reid and Graham (1996). However, as both the $^{3}He/^{4}He$ ratio and the crustal production ratio of the mantle would presumably have been higher in the past, the isolation periods calculated represent absolute maximum isolation times.

However, our results also advocate that closed system radiogenic ingrowth is not the only process required to account for mantle ratios measured. For the first time we have been able to resolve both the mantle He/Ne ratios and the He/Ar ratios of the SCLM source. Importantly, in both the Sheep Mountain and Bravo Dome fields, both of these isotope pairs are depleted relative to the MORB mantle values. This can only be explained by partial degassing of small melt fractions from asthenospheric melts that have been emplaced into the SCLM after radiogenic ingrowth.

6. Conclusions

We have identified that reduction of $^{3}He/^{4}He_{mantle}$ ratio within the Sheep Mountain gas field in central Colorado can be attributed to radiogenic production within the SCLM. Using a Reduced Chi-Squared minimisation on the variation of derived $^{4}He/^{21}Ne_{crust}$, combined with a radiogenically raised $^{21}Ne/^{22}Ne_{mantle}$ end member, we have resolved $^{3}He/^{4}He_{mantle}$ ratios of 2.59 ± 0.15 to 3.00 ± 0.18 R_a within the field. These values correspond with a $^{21}Ne/^{22}Ne_{mantle}$ value of 0.136. Using these resolved $^{3}He/^{4}He_{mantle}$ end member values with $^{21}Ne_{mantle}$ resolved from Ne three component analysis, has enabled a derivation of the elemental $^{3}He/^{22}Ne_{mantle}$ of 2.80 ± 0.16 and radiogenic $^{4}He/^{21}Ne^{*}_{mantle}$ range of 1.11 ± 0.11 to 1.30 ± 0.14. A second Reduced Chi-Squared minimisation performed on the variation of $^{21}Ne/^{40}Ar_{crust}$ ratios has allowed us to also determine both the $^{4}He/^{40}Ar_{mantle}$ range of 0.78 to 1.21 and $^{21}Ne/^{40}Ar_{mantle}$ of 7.66 ± 1.62 to 7.70 ± 1.54 within the field.

Using the known mantle production ranges for $^{4}He/^{21}Ne$ and $^{4}He/^{40}Ar$ has allowed us to determine the radiogenic He/Ne and He/Ar ratios that correspond to the radiogenically lowered $^{3}He/^{4}He_{mantle}$ ratios. Comparing these values with those resolved from both the Sheep Mountain field and the Bravo Dome field located in north western New Mexico by Ballentine et al. (2005) has allowed us to identify a clear and coherent depletion of He to Ne and He to Ar. This depletion can only be explained by partial degassing of small melt fractions from asthenospheric melts that have been emplaced into the SCLM. This is the first time that it has been possible to resolve and account for both the mantle He/Ne and He/Ar ratios within the SCLM source. We can also rule out the involvement of any plume component in the mantle source of the two gas fields and therefore also any plume influence on the Colorado Plateau Uplift event.

Acknowledgements

This research was supported by a UK Natural Environment Research Council (NERC) doctoral studentship and a subsequent postdoctoral grant (NE/C516479/1) and fellowship (NE/G015163/1) to S.M.V. Gilfillan. We thank BP and Larry Nugent for permission to sample at Sheep Mountain, Oxy for permission to sample Bravo Dome and Advanced Resources International, USA for their assistance in the field and in providing background information on the CO_2 reservoirs. Pete Burnard, Ray Burgess, Greg Holland, Mark Kendrick, Joanna Mount and David Murphy are also thanked for useful discussions on the topic. We appreciate the comments from two anonymous reviewers and editorial handling by Antonio Caracausi that greatly improved the manuscript.

References

Allis, R., Chidsey, T., Gwynn, W., Morgan, C., White, S., Adams, M., Moore, J., 2001. Natural CO_2 reservoirs on the Colorado Plateau and Southern Rocky Mountains: candidates for CO_2 sequestration. In: DOE/NETL: 1st National Conference of Carbon Sequestration, (Procedings Volume).

Baars, D.L., 2000. The Colorado Plateau: A Geologic History. University of New Mexico Press.

Baines, S.J., Worden, R.H., 2004. The long term fate of CO_2 in the subsurface: natural analogues for CO_2 storage. In: Bains, S.J., Worden, R.H. (Eds.), Geological Storage of Carbon Dioxide. Geological Society, London, pp. 59–85.

Ballentine, C.J., 1997. Resolving the mantle He/Ne and crustal $^{21}Ne/^{22}Ne$ in well gases. Earth Planet. Sci. Lett. 152, 233–249.

Ballentine, C.J., Burnard, P.G., 2002. Production, release and transport of noble gases in the continental crust. In: Porcelli, D.R., Ballentine, C.J., Weiler, R. (Eds.), Noble Gases in Geochemistry and Cosmochemistry, pp. 481–538.

Ballentine, C.J., Schoell, M., Coleman, D., Cain, B.A., 2001. 300-Myr-old magmatic CO_2 in natural gas reservoirs of the west Texas Permian basin. Nature 409, 327–331.

Ballentine, C.J., Burgess, R., Marty, B., 2002. Tracing fluid origin, transport and interaction in the crust. In: Porcelli, D.R., Ballentine, C.J., Weiler, R. (Eds.), Noble Gases in Geochemistry and Cosmochemistry, pp. 539–614.

Ballentine, C.J., Marty, B., Lollar, B.S., Cassidy, M., 2005. Neon isotopes constrain convection and volatile origin in the Earth's mantle. Nature 433, 33–38.

Barfod, D.N., Ballentine, C.J., Halliday, A.N., Fitton, J.G., 1999. Noble gases in the Cameroon line and the He, Ne, and Ar isotopic compositions of high μ (HIMU) mantle. J. Geophys. Res. Solid Earth 104, 29509–29527.

Barford, D.N., Ballentine, C.J., Halliday, A.N., Fitton, J.G., 1999. Noble gases in the Cameroon line and the He, Ne and Ar isotopic composition of high y (HIMU) mantle. J. Geophys. Res. 104, 29509–29527.

Becker, T.W., Faccenna, C., Humphreys, E.D., Lowry, A.R., Miller, M.S., 2014. Static and dynamic support of western United States topography. Earth Planet. Sci. Lett. 402, 234–246.

Beghoul, N., Barazangi, M., 1989. Mapping high Pn velocity beneath the Colorado Plateau constrains uplift models. J. Geophys. Res. Solid Earth Planets 94, 7083–7104.

Bianchi, D., Sarmiento, J.L., Gnanadesikan, A., Key, R.M., Schlosser, P., Newton, R., 2010. Low helium flux from the mantle inferred from simulations of oceanic helium isotope data. Earth Planet. Sci. Lett. 297, 379–386.

Bird, P., 1979. Continental delamination and the Colorado Plateau. J. Geophys. Res. Solid Earth 84, 7561–7571.

Boulos, M.S., Manuel, O.K., 1971. Xenon record of extinct radioactivities in earth. Science 174, 1334.

Bräuer, K., Kämpf, H., Niedermann, S., Strauch, G., 2013. Indications for the existence of different magmatic reservoirs beneath the Eifel area (Germany): a multi-isotope (C, N, He, Ne, Ar) approach. Chem. Geol. 356, 193–208.

Bräuer, K., Geissler, W.H., Kämpf, H., Niedermannn, S., Rman, N., 2016. Helium and carbon isotope signatures of gas exhalations in the westernmost part of the Pannonian Basin (SE Austria/NE Slovenia): evidence for active lithospheric mantle degassing. Chem. Geol. 422, 60–70.

Broadhead, R.F., 1998. Natural accumulations of carbon dioxide in the New Mexico region - where are they, how do they occur and what are the uses for CO_2? Lite Geol. 20, 2–6.

Burnard, P., Graham, D., Turner, G., 1997. Vesicle-specific noble gas analyses of "popping rock": implications for primordial noble gases in earth. Science 568–570.

Butler, W.A., Jeffery, P.M., Reynolds, J.H., 1963. Isotopic variations in terrestrial xenon. J. Geophys. Res. 68, 3283.

Caffee, M.W., Hudson, G.U., Velsko, C., Huss, G.R., Alexander, E.C., Chivas, A.R., 1999. Primordial noble gases from Earth's mantle: identification of a primitive volatile component. Science 285, 2115–2118.

Carroll, M.R., Draper, D.S., 1994. Noble gases as trace elements in magmatic processes. Chem. Geol. 117, 37–56.

Class, C., Goldstein, S.L., Stute, M., Kurz, M.D., Schlosser, P., 2005. Grand Comore Island: a well-constrained "low 3He/4He" mantle plume. Earth Planet. Sci. Lett. 233, 391–409.

Craig, H., Clarke, W.B., Beg, M.A., 1975. Excess 3He in deep water on the East Pacific Rise. Earth Planet. Sci. Lett. 26, 125–132.

Crovetto, R., Fernandez-Prini, R., Laura Japas, M., 1982. Solubilities of inert gases and methane in H_2O and in D_2O in the temperature range of 300 to 600 K. J. Chem. Phys. 76, 1077–1086.

Day, J.M.D., Hilton, D.R., 2011. Origin of 3He/4He ratios in HIMU-type basalts constrained from Canary Island lavas. Earth Planet. Sci. Lett. 305, 226–234.

Day, J.M.D., Hilton, D.R., Pearson, D.G., Macpherson, C.G., Kjarsgaard, B.A., Janney, P.E., 2005. Absence of a high time-integrated $^3He/(U + Th)$ source in the mantle beneath continents. Geology 33, 733–736.

Day, J.M.D., Barry, P.H., Hilton, D.R., Burgess, R., Pearson, D.G., Taylor, L.A., 2015. The helium flux from the continents and ubiquity of low-3He/4He recycled crust and lithosphere. Geochim. Cosmochim. Acta 153, 116–133.

Dilek, Y., Moores, E.M., 1999. A Tibetan model for the early Tertiary western United States. J. Geol. Soc. 156, 929–941.

Dodson, A., DePaolo, D., Kennedy, B., 1998. Helium isotopes in lithospheric mantle: evidence from Tertiary basalts of the western USA. Geochim. Cosmochim. Acta 62, 3775–3787.

Dunai, T.J., Baur, H., 1995. Helium, neon, and argon systematics of the European subcontinental mantle: implications for its geochemical evolution. Geochim. Cosmochim. Acta 59, 2767.

Dunai, T.J., Porcelli, D.R., 2002. Storage and transport of noble gases in the subcontinental lithosphere. In: Porcelli, D.R., Ballentine, C.J., Weiler, R. (Eds.), Noble Gases in Geochemistry and Cosmochemistry, pp. 371–409.

Duncan, R.A., Richards, M.A., 1991. Hotspots, mantle plumes, flood basalts and true polar wander. Rev. Geophys. 29, 31–50.

Erdman, M.E., Lee, C.-T.A., Levander, A., Jiang, H., 2016. Role of arc magmatism and lower crustal foundering in controlling elevation history of the Nevadaplano and Colorado Plateau: a case study of pyroxenitic lower crust from central Arizona, USA. Earth Planet. Sci. Lett. 439, 48–57.

Fitton, J.G., James, D., Leeman, W.P., 1991. Basic magmatism associated with Late Cenozoic extension in the western United-States - compositional variations in space and time. J. Geophys. Res. Solid Earth Planets 96, 13693–13711.

Gautheron, C., Moreira, M., 2002. Helium signature of the subcontinental lithospheric mantle. Earth Planet. Sci. Lett. 199, 39.

Gautheron, U., Moreira, M., Allegre, C., 2005. He, Ne and Ar composition of the European lithospheric mantle. Chem. Geol. 217, 97–112.

Gilfillan, S.M.V., Ballentine, C.J., Holland, G., Blagburn, D., Lollar, B.S., Stevens, S., Schoell, M., Cassidy, M., 2008. The noble gas geochemistry of natural CO_2 gas reservoirs from the Colorado Plateau and Rocky Mountain provinces, USA. Geochim. Cosmochim. Acta 72, 1174–1198.

Graham, D., 2002. Noble gas isotope geochemistry of mid-ocean ridge and ocean island basalt: characterization of mantle source reservoirs. In: Porcelli, D., Ballentine, C.J., Wieler, R. (Eds.), Noble Gases in Geochemistry and Cosmochemistry, pp. 247–317.

Hanyu, T., Kaneoka, I., 1997. The uniform and low 3He/4He ratios of HIMU basalts as evidence for their origin as recycled materials. Nature 390, 273–276.

Hanyu, T., Tatsumi, Y., Kimura, J.-I., 2011. Constraints on the origin of the HIMU reservoir from He–Ne–Ar isotope systematics. Earth Planet. Sci. Lett. 307, 377–386.

Hennecke, E.W., Manuel, O.K., 1975. Noble gases in CO_2 well gas, Harding County, New-Mexico. Earth Planet. Sci. Lett. 27, 346–355.

Holland, G., Ballentine, C.J., 2006. Seawater subduction controls the heavy noble gas composition of the mantle. Nature 441, 186–191.

Holland, G., Gilfillan, S.M.V., 2013. Application of noble gases to the viability of CO_2 storage. In: Burnard, P. (Ed.), The Noble Gases as Geochemical Tracers. Springer Berlin Heidelberg, Berlin, Heidelberg, pp. 177–223.

Honda, M., McDougall, I., 1998. Primordial helium and neon in the Earth—a speculation on early degassing. Geophys. Res. Lett. 25, 1951–1954.

Humphreys, E.D., 1995. Post-Laramide removal of the Farallon slab, western United States. Geology 23, 987–990.

Jalowitzki, T., Sumino, H., Conceição, R.V., Orihashi, Y., Nagao, K., Bertotto, G.W., Balbinot, E., Schilling, M.E., Gervasoni, F., 2016. Noble gas composition of subcontinental lithospheric mantle: an extensively degassed reservoir beneath Southern Patagonia. Earth Planet. Sci. Lett. 450, 263–273.

Jambon, A., Weber, H., Braun, O., 1986. Solubility of He, Ne, Ar, Kr and Xe in a basalt melt in the range 1250–1600 °C. Geochemical implications. Geochim. Cosmochim. Acta 50, 401–408.

Johnson, R.E., 1983. Bravo Dome carbon dioxide area, north east New Mexico. In: Fassett, J.E. (Ed.), Oil and Gas Fields of the Four Corners Area. Four Corners Geological Society, pp. 745–748.

Johnston, R.B., 1959. Geology of Huerferno Park Area, Huerferno and Custer County, Colorado. In: U.S. Geological Survey Bulletin No. 1071-D.

Kendrick, M.A., Scambelluri, M., Honda, M., Phillips, D., 2011. High abundances of noble gas and chlorine delivered to the mantle by serpentinite subduction. Nat. Geosci. 4, 807–812.

Kendrick, M.A., Honda, M., Pettke, T., Scambelluri, M., Phillips, D., Giuliani, A., 2013. Subduction zone fluxes of halogens and noble gases in seafloor and forearc serpentinites. Earth Planet. Sci. Lett. 365, 86–96.

Kipfer, R., Aeschbach-Gertig, W., Peeters, F., Stute, M., 2002. Noble gases in lakes and groundwaters. In: Noble Gases in Geochemistry and Cosmochemistry, pp. 615–700.

Levander, A., Schmandt, B., Miller, M.S., Liu, K., Karlstrom, K.E., Crow, R.S., Lee, C.T.A., Humphreys, E.D., 2011. Continuing Colorado plateau uplift by delamination-style convective lithospheric downwelling. Nature 472, 461–465.

Leya, I., Wieler, R., 1999. Nucleogeinc production of Ne isotopes in Earth's crust and upper mantle induced by alpha particles from the decay of U and Th. J. Geophys. Res. Solid Earth 104, 15439–15450.

Lux, G., 1987. The behavior of noble gases in silicate liquids: solution, diffusion, bubbles and surface effects, with applications to natural samples. Geochim. Cosmochim. Acta 51, 1549–1560.

Marty, B., Jambon, A., 1987. $C/^3He$ in volitile fluxes from the solid Earth: implications for carbon geodynamics. Earth Planet. Sci. Lett. 83, 16–26.

Matsumoto, T., Honda, M., McDougall, I., Reilly, S.Y., 1998. Noble gases in anhydrous lherzolites from the newer volcanics, southeastern Australia: a MORB-like reservoir in the subcontinental mantle. Geochim. Cosmochim. Acta 62, 2521.

Matsumoto, T., Chen, Y., Matsuda, J., 2001. Concomitant occurrence of primordial and recycled noble gases in the Earth's mantle. Earth Planet. Sci. Lett. 185 (1–2), 35–47. http://www.sciencedirect.com/science/article/pii/S0012821X00003757.

McDonough, W.F., 1990. Constraints on the composition of the continental lithospheric mantle. Earth Planet. Sci. Lett. 101, 1–18.

Miocic, J.M., Gilfillan, S.M.V., McDermott, C., Haszeldine, R.S., 2013. Mechanisms for CO_2 leakage prevention – a global dataset of natural analogues. Energy Procedia 40, 320–328.

Miocic, J.M., Gilfillan, S.M.V., Roberts, J.J., Edlmann, K., McDermott, C.I., Haszeldine, R.S., 2016. Controls on CO_2 storage security in natural reservoirs and implications for CO2 storage site selection. Int. J. Greenhouse Gas Control 51, 118–125.

Moreira, M., Kunz, J., Allegre, C., 1998. Rare gas systematics in popping rock: isotopic and elemental compositions in the upper mantle. Science 279, 1178–1181.

Moreira, M., Kanzari, A., Madureira, P., 2012. Helium and neon isotopes in São Miguel island basalts, Azores Archipelago: new constraints on the "low 3He" hotspot origin.

Chem. Geol. 322, 91–98.
Moucha, R., Forte, A.M., Rowley, D.B., Mitrovica, J.X., Simmons, N.A., Grand, S.P., 2008. Mantle convection and the recent evolution of the Colorado Plateau and the Rio Grande Rift valley. Geology 36, 439–442.
NETL, 2014. Subsurface Sources of CO2 in the Contiguous United States. Discovered Reservoirs, vol. 1 (DOE/NETL-2014/1637).
Parsons, T., McCarthy, J., 1995. The active southwest margin of the Colorado Plateau: uplift of mantle origin. Geol. Soc. Am. Bull. 107, 139–147.
Pearson, D.G., Wittig, N., 2008. Formation of Archaean continental lithosphere and its diamonds: the root of the problem. J. Geol. Soc. 165, 895–914.
Pearson, D.G., Carlson, R.W., Shirey, S.B., Boyd, F.R., Nixon, P.H., 1995a. Stabilisation of Archaean lithospheric mantle: a ReOs isotope study of peridotite xenoliths from the Kaapvaal craton. Earth Planet. Sci. Lett. 134, 341–357.
Pearson, D.G., Shirey, S.B., Carlson, R.W., Boyd, F.R., Pokhilenko, N.P., Shimizu, N., 1995b. Re–Os, Sm–Nd, and Rb–Sr isotope evidence for thick Archaean lithospheric mantle beneath the Siberian craton modified by multistage metasomatism. Geochim. Cosmochim. Acta 59, 959–977.
Phinney, D., Tennyson, J., Frick, U., 1978. Xenon in CO_2 well gas revisited. J. Geophys. Res., vol. 83 (5), 2313–2319. (10 May). http://onlinelibrary.wiley.com/doi/10.1029/JB083iB05p02313/abstract.
Porcelli, D.R., Ballentine, C.J., 2002. Models for the distribution of terrestrial noble gases and evolution of the atmosphere. In: Noble Gases in Geochemistry and Cosmochemistry, pp. 411–480.
Porcelli, D.R., Stone, J.O.H., O'Nions, R.K., 1987. Enhanced $^3He/^4He$ ratios and cosmogenic helium in ultramafic xenoliths. Chem. Geol. 64, 25.
Reid, M.R., Graham, D.W., 1996. Resolving lithospheric and sub-lithospheric contributions to helium isotope variations in basalts from the southwestern US. Earth Planet. Sci. Lett. 144, 213.
Roth, G., 1983. Sheep Mountain and Dike Mountain fields, Huerfano County, Colorado; a source of CO_2 for enhanced oil recovery. In: Fassett, J.E. (Ed.), Oil and Gas Fields of the Four Corners Area. Four Corners Geological Society, pp. 740–744.
Roy, M., Jordan, T.H., Pederson, J., 2009. Colorado Plateau magmatism and uplift by warming of heterogeneous lithosphere. Nature 459, 978–982.
Sathaye, K.J., Hesse, M.A., Cassidy, M., Stockli, D.F., 2014. Constraints on the magnitude and rate of CO2 dissolution at Bravo Dome natural gas field. Proc. Natl. Acad. Sci. 111, 15332–15337.
Seber, D., Barazangi, M., Ibenbrahim, A., Demnati, A., 1996. Geophysical evidence for lithospheric delamination beneath the Alboran Sea and Rif-Betic mountains. Nature 379, 785–790.
Smith, S.P., Reynolds, J.H., 1981. Excess ^{129}Xe in a terrestrial sample as measured in a pristine system. Earth Planet. Sci. Lett. 54, 236–238.
Staudacher, T., 1987. Upper mantle origin for harding county well gases. Nature 325, 605–607.
Sumino, H., Burgess, R., Mizukami, T., Wallis, S.R., Holland, G., Ballentine, C.J., 2010. Seawater-derived noble gases and halogens preserved in exhumed mantle wedge peridotite. Earth Planet. Sci. Lett. 294, 163–172.
Thompson, G.A., Zoback, M.L., 1979. Regional geophysics of the Colorado Plateau. Tectonophysics 61, 149–181.
Tucker, J.M., Mukhopadhyay, S., 2014. Evidence for multiple magma ocean outgassing and atmospheric loss episodes from mantle noble gases. Earth Planet. Sci. Lett. 393, 254–265.
Walker, R.J., Carlson, R.W., Shirey, S.B., Boyd, F.R., 1989. Os, Sr, Nd, and Pb isotope systematics of southern African peridotite xenoliths: implications for the chemical evolution of subcontinental mantle. Geochim. Cosmochim. Acta 53, 1583–1595.
White, R.S., McKenzie, D., 1995. Mantle plumes and flood basalts. J. Geophys. Res. 108, 17543–17585.
Wilson, J.T., 1973. Mantle plumes and plate motions. Tectonophysics 19, 149–164.
Woodward, L.A., 1983. Geology and hydrocarbon potential of the Raton Basin, New Mexico. In: Fassett, J.E. (Ed.), Oil and Gas Fields of the Four Corners Area. Four Corners Geological Society, pp. 789–799.
Yatsevich, I., Honda, M., 1997. Production of nucleogenic Ne in the earth from natural radioactive decay. J. Geophys. Res. Solid Earth 102, 10291–10298.
Zandt, G., Myers, S.C., Wallace, T.C., 1995. Crust and mantle structure across the Basin and Range Colorado Plateau boundary at 37-degrees-N latitude and implications for Cenozoic extensional mechanism. J. Geophys. Res. Solid Earth 100, 10529–10548.
Zartman, R.E., Reynolds, J.H., Wasserburg, G.J., 1961. Helium argon, and carbon in some natural gases. J. Geophys. Res. 66, 277–306.